Solar Energy 137 (2016) 143–147

Contents lists available at ScienceDirect

Solar Energy

journal homepage: www.elsevier.com/locate/solener

Pt-free spray coated reduced graphene oxide counter electrodes for dye sensitized solar cells

Charanadhar Nagavolu [a], K. Susmitha [b], M. Raghavender [b], L. Giribabu [c], Kota Bhanu Sankara Rao [d], C.T.G. Smith [e], C.A. Mills [e,f], S.R.P. Silva [e], V.V.S.S. Srikanth [a,*]

[a] School of Engineering Sciences and Technology, University of Hyderabad, Gachibowli, Hyderabad 500046, India
[b] Department of Physics, Yogi Vemana University, Kadapa 516003, India
[c] Inorganic and Physical Chemistry, Indian Institute of Chemical Technology, Hyderabad 500007, India
[d] Ministry of Steel Chair Professor, Department of Metallurgical and Materials Engineering, Mahatma Gandhi Institute of Technology, Hyderabad 500075, India
[e] Advanced Technology Institute, University of Surrey, Guildford, Surrey GU2 7XH, United Kingdom
[f] Tata Steel UK Ltd., 9 Sir William Lyon Road, University of Warwick Science Park, Coventry CV4 7EZ, United Kingdom

ARTICLE INFO

Article history:
Received 8 April 2016
Received in revised form 22 July 2016
Accepted 3 August 2016
Available online 11 August 2016

Keywords:
Graphene oxide
Reduced graphene oxide
Spray coating
Pt-free
Counter electrode
DSSC

ABSTRACT

Graphene oxide (GO) was synthesized using a modified Hummers method and was reduced by using focused sunlight to obtain solar reduced graphene oxide (SRGO). GO and SRGO are then used as Pt-free counter electrode materials in dye sensitized solar cells (DSSCs). GO and SRGO counter electrodes were prepared by a simple spray coating method to produce homogeneous electrode layers. The DSSCs with GO and SRGO counter electrodes exhibited an overall power conversion efficiencies of ~3.4 and ~4%, respectively. Cyclic voltammetry and electrochemical impedance spectroscopy reveal that the DSSC with SRGO counter electrode exhibits higher electro-catalytic activity and lower charge transfer resistance at the electrode/electrolyte interface (in comparison to the DSSC with GO) resulting in higher conversion efficiency. Moreover, the microstructural features of SRGO are found to be suitable for its improved interaction with the liquid electrolyte and the enhanced electro-catalytic activity at its surface.

1. Introduction

Gratzel cells or *Dye Sensitized Solar Cells* (DSSCs) (O'Regan and Grätzel, 1991; Grätzel, 2003; Imalka Jayawardena et al., 2013) are expected to challenge the performance of Si based solar cells and compete for a significant market share in next generation solar cells. This is owing to their good performance even under diffuse light (Cornaro and Andreotti, 2013), lower production costs, innate solution processability which allows easy fabrication of large area cells, and excellent unit price per performance metric which allows them to gain grid parity. A DSSC typically consists of a photo-anode, an electrolyte with redox species (such as iodide/tri-iodide (I^-/I_3^-) in an organic solvent), and a counter electrode (CE). The anode consists of a transparent conducting oxide (TCO) coated glass substrate with a layer of mesoporous network of wide band gap metal oxide semiconductor, such as TiO_2, which is sensitized with a suitable dye. The redox couple in the electrolyte works as a mediator which transfers electrons from the cathode to the oxidized dye molecules (Wu et al., 2015). I^- ions reduce the sensitizer and oxidize to I_3^- ions while the monovalent I^- ions are recovered at the cathode.

Commonly, platinum coated TCO glass substrate is used as the CE because of platinum's high catalytic activity and resistance to corrosion due to the electrolyte. However, due to platinum's high cost and low corrosion resistance to the iodide based electrolytes (Koo et al., 2006; Agresti et al., 2015), scientists have investigated alternative CEs and redox couple electrolytes other than iodide/tri-iodide (I^-/I_3^-). These alternative electrolytes, such as anion doped PEDOT (Xia et al., 2008), have assisted in producing stable solid state DSSCs. Instead of Pt, a number of carbon based materials (Janani et al., 2015) including graphene related materials (Choi et al., 2011; Wang and Hu, 2012; Gong et al., 2012; Yeh et al., 2014; Zhu et al., 2015; Huo et al., 2016) have been tested as alternative CE materials which exhibited excellent conductivity and high electro-catalytic activity. Even though the efficiencies of DSSCs with graphene related materials (graphene obtained through electrophoretic deposition (Choi et al., 2011) and graphene with incorporation of SiO_2 nanoparticles (Gong et al., 2012)) as CE materials are high (5.69% (Choi et al., 2011) and 4.04% (Gong et al., 2012)), the fabrication of devices involve complex process steps and therefore require optimization of a number

* Corresponding author.
E-mail address: vvsssse@uohyd.ernet.in (V.V.S.S. Srikanth).

http://dx.doi.org/10.1016/j.solener.2016.08.002
0038-092X/

of process parameters. In another important work (Yeh et al., 2014) the efficiency of DSSC with photothermal reduced graphene oxide (P-rGO) as CE was 7.62%, the method used for fabricating the final CE may not be suitable for realizing large area CEs. In the case of graphene based composites as CE materials in DSSCs, it is difficult to understand and control the electrochemical activity at the electrode/electrolyte interface. However, graphene ink (Casaluci et al., 2016) spray coated on FTO substrates was recently used as a CE in fabricating large-area DSSC modules via the spray coating technique. In this case, the electrochemical activity at the electrode/-electrolyte interface could be easily explained. Additionally, using a CE composed of graphene nanoplatelets (GNP), in the structure FTO/Au/GNP, produced a DSSC with a record efficiency of over 14% (Kakiage et al., 2015), outperforming a similar FTO/Pt CE DSSC. In both cases, the electrolyte was a cobalt(III/II) tris(1,10-phenanthroline) complex ($[Co(phen)^{3+/2+}]$) transition metal redox couple system with TiO_2 electrodes co-photosensitised with a strongly anchored alkoxysilyl-dye (ADEKA-1) and a carboxy-organic dye (LEG4).

On the contrary to the above mentioned works, in this work we have demonstrated an easy fabrication process of robust DSSCs with graphene oxide (GO) and solar reduced graphene oxide (SRGO) as CE materials and nanocrystalline TiO_2 photo-anode. The novel points of this work are: (i) integrating an excellent photo-anode (Susmitha et al., 2015) into DSSC, (ii) easy and renewable method of preparing CE materials without any metallic layer or in composite form, (iii) spray coating of CE materials facilitating the fabrication of large area CEs, (iv) energy conversion efficiency of ~4% (without using Pt or any CE material in composite form), comparable to the values exhibited by DSSCs with graphene composites and (v) owing to the innate nature of the CE materials used in this work, the electrochemical activity at the electrode/electrolyte interface could be easily explained.

2. Experimental details

2.1. Preparation of nanocrystalline TiO_2 photo-anode

Photo-electrodes were fabricated by following a previously reported procedure (Susmitha et al., 2015) which is briefly given here for convenience. As-procured fluorine-doped tin oxide (FTO) conducting glass plates (7 Ω/square, TCO22-7, Solaronix) were cleaned with a detergent solution and then rinsed sequentially with Millipore water, absolute ethanol and 2-propanol (Merck, Germany) to remove organic and other particulate contaminants. FTO glass plates where then dried under a nitrogen purge. Nanocrystalline titanium dioxide (TiO_2, anatase phase) layer was coated onto the FTO glass plates and then sintered. In order to make sure that the TiO_2 layer has a good mechanical contact with the conducting FTO glass substrate, TiO_2 coated plates were treated with a 40 mM titanium tetrachloride ($TiCl_4$) solution at 70 °C. A 43T mesh screen was used to produce ~12 μm thick TiO_2 film using commercial 18 nm TiO_2 colloidal paste (18NR-T, Dyesol) after sintering at 500 °C for 30 min. Another 90T mesh screen was used to produce ~6 μm thick film of 200 nm scatter TiO_2 paste (WER2-O, Dyesol). A post-deposition $TiCl_4$ treatment was then undertaken, before sintering further at 500 °C for 30 min. While cooling the electrodes to around 110 °C, the electrodes were stained in purified cis–bis (isothiocyanato) bis (2,2′-bipyridyl-4,4′-dicarboxylato) ruthenium (II)–bis-tetrabutylammonium dye solution (0.3 mM, N719), prepared in a mixture of tert-butanol/acetonitrile (1/1 v/v), for 18 h under dark conditions. The photo-electrode was subsequently withdrawn from the solution and rinsed twice with anhydrous acetonitrile to remove any unanchored dye molecules on the surface of the TiO_2 film. The plates were finally dried under nitrogen purge.

2.2. Fabrication of GO and SRGO CEs

GO and SRGO were prepared using previously reported procedures (please see supporting information (SI) for details) (Gedela et al., 2015). 1 mg of GO (or SRGO) was then dispersed in 1 mL of iso-propanol (Merck, Germany) and the resultant solution was ultrasonicated for 30 min prior to spray coating the entire volume with a spray gun at 1 mL/min using pure N_2 gas. To inject the electrolyte into the test cells, holes (0.1 mm diameter) were drilled into the FTO glass plates using a micro-tipped drill (DREMEL 300) with a diamond coated micro-drill bit. The FTO glass was washed sequentially with diluted detergent, 0.1 M HCl solution in ethanol, Millipore water, absolute ethanol and finally cleaned with iso-propanol in a sonicator for 30 min. The cleaned FTO glass substrate was placed on a hotplate at 180 °C and the entire 1 ml of GO (or SRGO) solution was spray coated using a 0.3 mm micro-tip needle spray gun at 1 mL min^{-1} using pure N_2 gas. The temperature 180 °C was used during spray coating to ensure the evaporation of the solvent and good adhesion of the GO (or SRGO) to the FTO substrate. The heat treatment to a moderate temperature of 380 °C after the coating is to increase the porosity of GO (or SRGO) for enhancing the adsorption of the electrolyte for improvement in electrochemical activity, which in turn enhances the efficiency of the DSSC. The spray coated GO or SRGO FTO glass substrate was then heated in a furnace at 380 °C for 30 min to obtain FTO/GO and FTO/SRGO CEs.

2.3. Fabrication of DSSCs

The photo-anodes and CEs were assembled using thermal adhesive (25 μm, Surlyn, Solaronix) as a spacer to produce a sandwich cell. The liquid electrolyte was prepared by mixing 1-butyl-3-methylimidazoliumiodide (BMII, 0.5 M), lithium iodide (LiI, 0.1 M), Iodine (I_2, 0.05 M), guanidinethiocyanate (GuNC, 0.1 M), and ter-butylpyridine (tBP, 0.5 M) in acetonitrile. The prepared electrolyte was injected through the hole drilled through the CE, before the holes were sealed with a cover glass using Surlyn. The fabricated DSSCs (Table 1) have an active area of ~0.36 cm^2.

2.4. Electrochemical characterization and DSCC testing

Cyclic-voltammetry was used to understand $I^- - I_3^-$ redox reaction occurring in the $LiClO_4$ (0.1 M)/LiI (5 mM)/I_2 (0.5 mM)/ acetonitrile electrolyte solution at the CEs. A potentiostat (CHI608E instrument) in a three electrode configuration was used to measure the current at a scan rate of 10 mV s^{-1}. An Ag/Ag^+ electrode (0.01 M $AgNO_3$ in acetonitrile) was used as the reference electrode, and the TiO_2/dye complex was used as the working electrode. Electrochemical impedance spectroscopy (EIS) was performed in the frequency range of 0.1 Hz to 100 kHz on an electrochemical workstation (IVIUMSTAT, IVIUM technologies b.v.) at 10 mV and respective open circuit voltage.

To check the solar photovoltaic performance of the fabricated DSSCs, the current density-voltage characteristics were measured under the illumination of Xe arc solar simulator (PEC-L01, Peccell

Table 1
Photo- and counter- electrode configurations.

Photo-electrode	Counter electrode	Cell name
FTO/TiO_2/N719	FTO/GO	GO-DSSC
FTO/TiO_2/N719	FTO/SRGO	SRGO-DSSC

Inc., Japan) with AM 1.5 spectral filter and source-meter (2401 Keithley Instruments Inc, U.S.A.). The intensity was adjusted to provide 1 sun (100 mW cm^{-2}) using a calibrated Si solar cell. The power conversion efficiency (η) was calculated using Eq. (1)

$$\eta = \frac{FF \times V_{OC} \times J_{SC}}{P_{in}} \quad (1)$$

while the fill factor (FF) was calculated using Eq. (2)

$$FF = \frac{V_{max} \times I_{max}}{V_{OC} \times J_{SC}} \quad (2)$$

where P_{in} is the input power density (i.e., the intensity of incident light in mW/cm^2), V_{OC} is the open-circuit voltage (mV), J_{SC} is the short-circuit current density (mA/cm^2) and V_{max} and I_{max} are the voltage and current at maximum power output, respectively.

3. Results and discussion

X-ray diffraction (XRD) analysis of graphite flakes (the starting material), GO and SRGO showed characteristic differences in the diffraction peak positions confirming the formation of GO from graphite flakes and SRGO from GO. X-ray diffractogram of SRGO indicates that the reduction of GO to SRGO is only partial and therefore, the residual oxygen functional groups present in the case of SRGO may assist in enhanced wetting of the SRGO by the liquid electrolyte and participate in the intercalation and adsorption of cations onto SRGO while participating in the operation of DSSC. This indicates that SRGO may perform better than GO as a CE in DSSC. Raman scattering analysis complemented well with the XRD analysis. Electron microscopy showed that SRGO consisted of randomly aggregated, thin and wrinkled graphene sheets with a close restacking with one another forming a disordered solid. SRGO exhibited mesoporosity which can play a major role in enhancing its performance as a CE as it allows the faster mobility of the charge carriers and thereby improving the activity at the electrode/electrolyte interfacial area. N_2 adsorption/desorption isotherms of GO and SRGO resembled type IV characteristics of Brunauer-Emmett-Teller (BET) classification types I-VI whilst the hysteresis loops in both the cases are found in the relative pressure range of 0.4–0.9. BET specific surface area of SRGO (~107 m^2/g) was found to be more than double that of GO (~51 m^2/g). Please see SI for the detailed discussion on different characteristics of GO and SRGO (Gedela et al., 2015).

In literature, cobalt mediator is normally used instead of iodine based mediator to obtain good performance. Although cobalt redox couples have been shown to produce exemplary DSSC efficiencies (Kakiage et al., 2015), it is reported in the literature that the Co (II)/Co(III) redox couple is not compatible with Ru metallorganic (or other metal cation) sensitizers (Polander et al., 2013), possibly due to enhanced recombination (Liu et al., 2011). Hence, in the present study, an iodine mediator electrolyte is used due to the fabrication of the DSSCs using the Ru-based N719 dye. The main functions of a CE in DSSC are to provide the pathway for electron transfer from the external circuit to the redox electrolyte and to catalyze the reduction of I_3^- to promote the regeneration of dye molecules (Yen et al., 2011; Jang et al., 2012; Beliatis et al., 2014). Therefore, the electro-catalytic activity during the reduction of I_3^- is a key factor for determining the performance of a CE. In this context, CV curves of GO and SRGO are compared in Fig. 1. Two redox peaks are discernible in the case of SRGO electrode. The peak at ~ 0.64 V is attributed to $3I_2 + 2e^- \rightarrow 2\ I_3^-$ reaction whilst the one at ~0.79 V is attributed to $I_3^- + 2e^- \rightarrow 3I^-$ reaction (Wu et al., 2011). On the other hand, a lone cathodic peak at ~0.59 V is discernible in the case of GO electrode. Peaks corresponding to redox pairs (as observed in the case of SRGO) are indiscernible probably due to the domination of background current. CV characteristics of GO and SRGO electrodes as-extracted from the CV curves are compared in Table 2. The smaller difference (ΔE_p) between the cathodic and anodic peak potentials in the case of SRGO electrode in comparison to that of GO electrode shows that SRGO is a better electrode to catalyze the reduction of the triiodide ion to iodide.

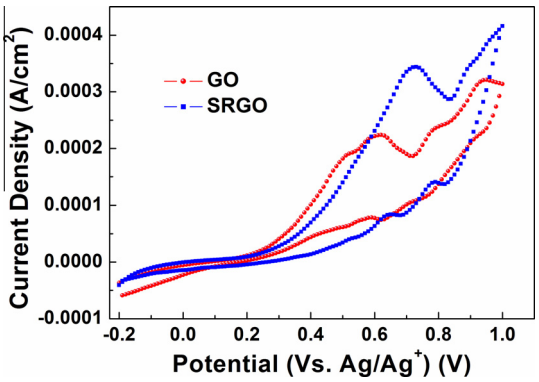

Fig. 1. CV curves of GO and SRGO electrodes.

Nyquist plots pertaining to DSSCs constituted by GO and SRGO CEs are shown in Fig. 2. The circuit (as-obtained by fitting the EIS data using the software IVIUM Soft v. 2.509) corresponding to the spectra is also shown in Fig. 2. The sheet resistance element (R_s) of the GO and SRGO DSSCs is measured as 49 and 5 Ω cm^2 respectively, indicating that the SRGO film is firmly bonded to the FTO substrate and exhibits a lower R_s and therefore indicating an enhanced electron transfer from SRGO CE to the I_3^- ion in the electrolyte. The lower internal resistance element (R_{ct1}) measured as ~34 Ω cm^2 at the SRGO CE/electrolyte interface (compared to ~175 Ω cm^2 in the case of GO) indicates that an enhanced electro-catalytic redox reactivity is achieved in the reduction of I_3^- at the interface. Low R_s and total internal resistance (R_{ct}) are indicative of the ease of transfer of charge to the CE and effective reduction of I_3^- to I^- at the electrolyte/CE interface, respectively and both of which favour the regeneration of the dye molecules at the electrolyte/photoelectrode interface (Dürr et al., 2006). Lower R_{ct} also means a lower over-potential for electrons transferring from CE to electrolyte, and is therefore also indicative of an easier electron transfer (Papageorgiou et al., 1997; Yoon et al., 2008; Zhou et al., 2009). It is known that the lower R_s and R_{ct1} values subsequently lead to an enhancement in J_{SC} (Hou et al., 2013). The photocurrent density (J) versus voltage (V) curves of the fabricated DSSCs are shown in Fig. 3 while the calculated photovoltaic parameters of the cells are tabulated in Table 3.

The S-shaped JV curves (Fig. 3) arise due to charge accumulation/trapping at either of the electrode electrolyte interfaces as a result of a mismatch between the work function and the electrolyte redox potentials (Sundqvist et al., 2016). This is more likely to occur at the FTO/TiO_2 cathode, due to the unavoidable existence

Table 2
Comparison of CV characteristics of GO and SRGO electrodes.

Sample	Peak potential (mV)			ΔE_p (mV)
	Cathodic	Anodic	Reaction	
GO	–	590	–	–
	720	690	$3I_2 + 2e^- \rightarrow 2I_3^-$	30
	890	830	$I_3^- + 2e^- \rightarrow 3I^-$	60
SRGO	520	520	–	0
	620	640	$3I_2 + 2e^- \rightarrow 2I_3^-$	20
	790	780	$I_3^- + 2e^- \rightarrow 3I^-$	10

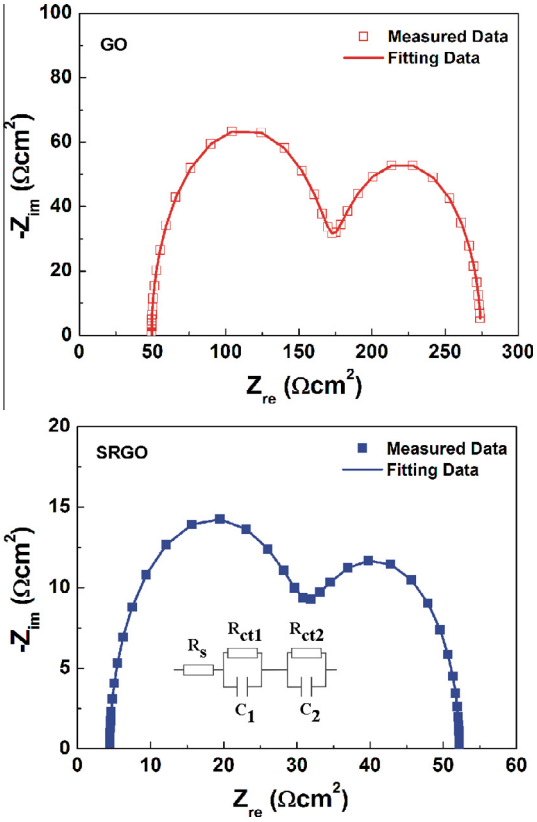

Fig. 2. Electrochemical impedance spectra of GO and SRGO. Inset shows the equivalent circuit used for fitting the EIS data in both GO and SRGO cases.

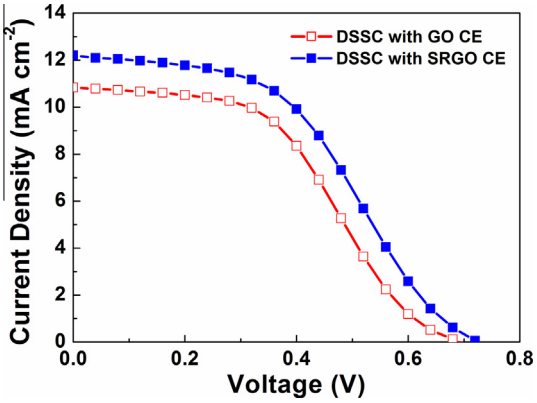

Fig. 3. Photocurrent density versus voltage characteristics of different DSSCs.

Table 3
Comparison of the photovoltaic performance of the GO and SRGO DSSC test cells.

Cell name	V_{OC} (V)	J_{SC} (mA/cm^2)	*FF*	η (%)	R_s (Ω cm^2)	R_{ct} (Ω cm^2)
GO-DSSC	0.69	10.83	0.45	3.38	49.02	175
SRGO-DSSC	0.72	12.20	0.44	3.96	5.04	34

of impurity induced energy gap states in the thin TiO_2 layer and the low mobility of holes during charge transport due to their hopping mechanism. Alternatively, it may be due to defects at the counter electrode interface, and other interfacial behavior in the fabricated solar cells (De Castro et al., 2010; Tress et al., 2011; Wagner et al., 2012).

The DSSC with SRGO CE exhibits J_{SC} of 12.20 mA/cm^2, V_{OC} of 0.72 V and *FF* of 0.44. This yields η of 3.96%, which is higher than that of the DSSC constituted by GO CE (η = 3.38%). The higher V_{OC} in the case of SRGO is attributed to the positive shift in the iodide/tri-iodide redox energy level (Dürr et al., 2006; Zhou et al., 2009).

4. Conclusions

In this work, GO and SRGO were synthesized using easy methods and the as-synthesized materials are spray coated onto FTO glass substrates which were then used as CEs in DSSCs. In other words, Pt-free CEs were fabricated and used in DSSCs. The fabrication process used in this work to obtain DSSCs is not a complicated process in comparison to the other works in the literature. SRGO exhibited a more suitable electrochemical behavior than GO. The conversion efficiencies obtained in this work when GO and SRGO CEs are used in DSSCs are 3.38 and 3.96%, respectively.

Acknowledgments

The authors (C.N, C.A.M, S.R.P.S, K.B.S.R and V.V.S.S.S) acknowledge The Department of Science and Technology (DST), India, and the British Council, UK, for their financial support through the UK-India Education and Research Initiative (UKIERI) (project no. DST/INT/UK/P-76/2014). M.R greatly acknowledges DST, India, for the financial support through the sanctioned project (project no. SR/FTP/PS-111/2010). The authors thank Dr. Imalka Jayawardena (Advanced Technology Institute, University of Surrey) for helpful discussions.

Appendix A. Supplementary material

Supplementary data associated with this article can be found, in the online version, at http://dx.doi.org/10.1016/j.solener.2016.08.002.

References

Agresti, A., Pescetelli, S., Gatto, E., Venanzi, M., Di Carlo, A., 2015. Polyiodides formation in solvent based Dye Sensitized Solar Cells under reverse bias stress. J. Power Sources 287, 87–95.
Beliatis, M.J., Gandhi, K.K., Rozanski, L.J., Rhodes, R., McCafferty, L., Alenezi, M.R., Alshammari, A.S., Mills, C.A., Jayawardena, K.D.G.I., Henley, S.J., Silva, S.R.P., 2014. Hybrid graphene-metal oxide solution processed electron transport layers for large area high-performance organic photovoltaics. Adv. Mater. 26, 2078–2083.
Casaluci, S., Gemmi, M., Pellegrini, V., Di Carlo, A., Bonaccorso, F., 2016. Graphene-based large area dye-sensitized solar cell modules. Nanoscale 8, 5368–5378.
Choi, H., Kim, H., Hwang, S., Han, Y., Jeon, M., 2011. Graphene counter electrodes for dye-sensitized solar cells prepared by electrophoretic deposition. J. Mater. Chem. 21, 7548–7551.
Cornaro, C., Andreotti, A., 2013. Influence of Average Photon Energy index on solar irradiance characteristics and outdoor performance of photovoltaic modules. Prog. Photovolt.: Res. Appl. 21, 996–1003.
De Castro, F.A., Heier, J., Nesch, F., Hany, R., 2010. Origin of the kink in current-density versus voltage curves and efficiency enhancement of polymer-C 60 heterojunction solar cells. IEEE J. Sel. Top. Quantum Electron. 16, 1690–1699.
Dürr, M., Yasuda, A., Nelles, G., 2006. On the origin of increased open circuit voltage of dye-sensitized solar cells using 4-tert-butyl pyridine as additive to the electrolyte. Appl. Phys. Lett. 89, 061110.
Gedela, V., Puttapati, S.K., Nagavolu, C., Srikanth, V.V.S.S., 2015. A unique solar radiation exfoliated reduced graphene oxide/polyaniline nanofibers composite electrode material for supercapacitors. Mater. Lett. 152, 177–180.
Gong, F., Li, Z., Wang, H., Wang, Z.-S., 2012. Enhanced electrocatalytic performance of graphene via incorporation of SiO_2 nanoparticles for dye-sensitized solar cells. J. Mater. Chem. 22, 17321–17327.
Grätzel, M., 2003. Dye-sensitized solar cells. J. Photochem. Photobiol. C: Photochem. Rev. 4, 145–153.
Hou, S., Cai, X., Wu, H., Yu, X., Peng, M., Yan, K., Zou, D., 2013. Nitrogen-doped graphene for dye-sensitized solar cells and the role of nitrogen states in triiodide reduction. Energy Environ. Sci. 6, 3356–3362.

Huo, J., Wu, J., Zheng, M., Tu, Y., Lan, Z., 2016. A transparent cobalt sulfide/reduced graphene oxide nanostructure counter electrode for high efficient dye-sensitized solar cells. Electrochim. Acta 187, 210–217.

Imalka Jayawardena, K.D.G., Rozanski, L.J., Mills, C.A., Beliatis, M.J.N., Nismya, A., Silva, S.R.P., 2013. 'Inorganics-in-Organics': recent developments and outlook for 4G polymer solar cells. Nanoscale 5, 8411–8427.

Janani, M., Srikrishnarka, P., Nair, S.V., Nair, A.S., 2015. An in-depth review on the role of carbon nanostructures in dye-sensitized solar cells. J. Mater. Chem. A 3, 17914–17938.

Jang, H.-S., Yun, J.-M., Kim, D.-Y., Park, D.-W., Na, S.-I., Kim, S.-S., 2012. Moderately reduced graphene oxide as transparent counter electrodes for dye-sensitized solar cells. Electrochim. Acta 81, 301–307.

Kakiage, K., Aoyama, Y., Yano, T., Oya, K., Fujisawa, J., Hanaya, M., 2015. Highly-efficient dye-sensitized solar cells with collaborative sensitization by silyl-anchor and carboxy-anchor dyes. Chem. Commun. 51, 15894–15897.

Koo, B.-K., Lee, D.-Y., Kim, H.-J., Lee, W.-J., Song, J.-S., Kim, H.-J., 2006. Seasoning effect of dye-sensitized solar cells with different counter electrodes. J. Electroceram. 17, 79–82.

Liu, Y., Jennings, J.R., Huang, Y., Wang, Q., Zakeeruddin, S.M., Grätzel, M., 2011. Cobalt redox mediators for ruthenium-based dye-sensitized solar cells: a combined impedance spectroscopy and near-IR transmittance study. J. Phys. Chem. C 115, 18847–18855.

O'Regan, B., Grätzel, M., 1991. A low-cost, high-efficiency solar cell based on dye-sensitized colloidal TiO_2 films. Nature 353, 737–740.

Papageorgiou, N., Maier, W.F., Grätzel, M., 1997. An iodine/triiodide reduction electrocatalyst for aqueous and organic media. J. Electrochem. Soc. 144, 876–884.

Polander, L.E., Yella, A., Curchod, B.F.E., Ashari Astani, N., Teuscher, J., Scopelliti, R., Gao, P., Mathew, S., Moser, J.E., Tavernelli, I., Rothlisberger, U., Grätzel, M., Nazeeruddin, M.K., Frey, J., 2013. Towards compatibility between ruthenium sensitizers and cobalt electrolytes in dye-sensitized solar cells. Angew. Chem. Int. Ed. 52, 8731–8735.

Sundqvist, A., Sandberg, O.J., Nyman, M., Smått, J., Österbacka, R., 2016. Origin of the S-shaped JV curve and the light-soaking issue in inverted organic solar cells. Adv. Energy Mater. 6, 1502265.

Susmitha, K., Naresh Kumar, M., Rajkumar, G., Giribabu, L., Raghavender, M., 2015. Enhanced dye sensitized solar cell performance with high surface area thin ZnO film and PEDOT:PSS. Sol. Energy 118, 126–133.

Tress, W., Leo, K., Riede, M., 2011. Influence of hole-transport layers and donor materials on open-circuit voltage and shape of I-V curves of organic solar cells. Adv. Funct. Mater. 21, 2140–2149.

Wagner, J., Gruber, M., Wilke, A., Tanaka, Y., Topczak, K., Steindamm, A., Hörmann, U., Opitz, A., Nakayama, Y., Ishii, H., Pflaum, J., Koch, N., Brütting, W., 2012. Identification of different origins for s-shaped current voltage characteristics in planar heterojunction organic solar cells. J. Appl. Phys. 111, 054509.

Wang, H., Hu, Y.H., 2012. Graphene as a counter electrode material for dye-sensitized solar cells. Energy Environ. Sci. 5, 8182–8188.

Wu, M., Zhang, Q., Xiao, J., Ma, C., Lin, X., Miao, C., He, Y., Gao, Y., Hagfeldt, A., Ma, T., 2011. Two flexible counter electrodes based on molybdenum and tungsten nitrides for dye-sensitized solar cells. J. Mater. Chem. 21, 10761–10766.

Wu, J., Lan, Z., Lin, J., Huang, M., Huang, Y., Fan, L., Luo, G., 2015. Electrolytes in dye-sensitized solar cells. Chem. Rev. 115, 2136–2173.

Yeh, M.H., Lin, L.Y., Chang, L.Y., Leu, Y.A., Cheng, W.Y., Lin, J.J., Ho, K.C., 2014. Dye-sensitized solar cells with reduced graphene oxide as the counter electrode prepared by a green photothermal reduction process. Chem. Phys. Chem. 15 (6), 1175–1181.

Yen, M.-Y., Teng, C.-C., Hsiao, M.-C., Liu, P.-I., Chuang, W.-P., Ma, C.-C.M., Hsieh, C.-K., Tsai, M.-C., Tsai, C.-H., 2011. Platinum nanoparticles/graphene composite catalyst as a novel composite counter electrode for high performance dye-sensitized solar cells. J. Mater. Chem. 21, 12880–12888.

Yoon, C.H., Vittal, R., Lee, J., Chae, W.-S., Kim, K.-J., 2008. Enhanced performance of a dye-sensitized solar cell with an electrodeposited-platinum counter electrode. Electrochim. Acta 53, 2890–2896.

Xia, J., Masaki, N., Lira-cantu, M., Kim, Y., Jiang, K., Yanagida, S., 2008. Influence of doped anions on poly (3,4-ethylenedioxythiophene) as hole conductors for iodine-free solid-state dye-sensitized solar cells. J. Am. Chem. Soc. 130, 1258–1263.

Zhou, C.-H., Yang, Y., Zhang, J., Xu, S., Wu, S.-J., Hu, H., Chen, B.-L., Tai, Q.-D., Sun, Z.-H., Zhao, X.-Z., 2009. Enhanced electrochemical performance of the counter electrode of dye sensitized solar cells by sandblasting. Electrochim. Acta 54, 5320–5325.

Zhu, C., Min, H., Xu, F., Chen, J., Dong, H., Tong, L., Zhu, Y., Sun, L., 2015. Ultrafast electrochemical preparation of graphene/CoS nanosheet counter electrodes for efficient dye-sensitized solar cells. RSC Adv. 5, 85822–85830.